INTERNATIONAL JOURNAL FOR NUMERICAL METHODS IN FLUIDS
Int. J. Numer. Meth. Fluids 2012; **68**:1102–1125
Published online 25 May 2011 in Wiley Online Library (wileyonlinelibrary.com). DOI: 10.1002/fld.2594

The computation of the eddy along the upper wall in the three-dimensional flow over a backward-facing step

N. A. Malamataris[1,2,*,†] and R. Löhner[1]

[1] *Center for Computational Fluid Dynamics, Department of Computational and Data Sciences, George Mason University, Fairfax, VA 22030, USA*
[2] *TEI of W. Macedonia, Kila-Kozani 50100, Greece*

SUMMARY

A three-dimensional laminar flow over a backward-facing step is studied as a numerical experiment by solving the steady-state, isothermal and incompressible Navier–Stokes equations using two different finite element codes. The Reynolds number ranges from 100 to 1050. The expansion ratio is 1:1.94, and the aspect ratio is 1:36.7. The numerical experiment reveals both eddies along the lower and upper walls downstream of the step. Results of computations regarding positions of detachment of the eddy along the upper wall and positions of reattachments of the eddies along both the lower and upper walls are tabulated along with positions and magnitudes of global extrema of shear rate within the eddies. The wall effects are shown by calculating streamlines along planes parallel/normal to the lateral walls of the domain and depicting how the streamlines are distorted close to the walls and how they assume a two-dimensional configuration in the plane of symmetry. Comparisons are made with available numerical results and laboratory measurements.

Received 12 October 2010; Revised 13 February 2011; Accepted 26 March 2011

KEY WORDS: 3D backward-facing step; wall effects; eddies along upper and lower walls; finite elements; separated flows

1. INTRODUCTION

A backward-facing step is a fundamental flow in fluid mechanics that has served as a test case for laboratory techniques and numerical methods. In addition, this flow is a case example of a separated flow that is being used in a study of complex dynamic phenomena of transition, stability, and so on. A thorough recent review on that subject may be found in the work of Schäfer *et al.* [1].

This flow has even been a leading example in a direct numerical simulation of turbulence [1, 2]. However, there is a lack in the literature of a three-dimensional computational study that can predict with acceptable accuracy the relatively complex separation phenomena in the laminar regime by using a computational domain with the same dimensions as the test section of an actual laboratory experiment. The main aim of this work is to fill in this gap.

The physics of the laminar backward-facing step flow are well understood because of the pioneering work of Armaly *et al.* [3]. This fact has been acknowledged in relevant reviews early on (e.g., Adams and Johnston [4, p. 494]) In addition, their experiments have been verified by Lee and Mateescu [5] and Tylli *et al.* [6] who used similar expansion and aspect ratios. Finally, the two eddies (a primary eddy along a lower wall and a secondary eddy along an upper wall) that appear in this flow for $Re > 400$ have been predicted by all authors who have performed two-dimensional computations in the laminar flow regime (e.g., Erturk [7] for the latest review).

*Correspondence to: N. A. Malamataris, 4400 University Dr. MSN 6A2, Fairfax, VA 22030, USA.
†E-mail: nmalamat@gmu.edu

Armaly *et al.* [3] have reported three-dimensional effects in their measurements although they have used an aspect ratio of 1:36.7 (the ratio of step span to step height). This choice was on the safe side of a suggested aspect ratio of 1:30, which guarantees two-dimensional results in the plane of symmetry according to De Brederode and Bradshaw [8, p. 33]. In the literature, the three-dimensional effects of the experiments by Armaly *et al.* [3] have been explained according to Schäfer *et al.* [1, p. 87] in the work of Williams and Baker [9]. Indeed, Williams and Baker [9, p. 1166] predicted very well the primary eddy in their three-dimensional computations by using the test section of Armaly *et al.* [3] as their computational domain. Regarding the computation of the eddy along the upper wall, they briefly mentioned in their text (p. 1169 of their work) that it appears short in the plane of symmetry, and they avoided any comparison with the experimental data.

Clearly, a full three-dimensional numerical experiment over a backward-facing step in the laminar regime, which predicts with satisfactory accuracy both eddies of this flow, may shed more light in the interpretation of the results of Armaly *et al.* [3] . This is the second aim of this work.

All three-dimensional computational approaches so far successfully predict the primary eddy along the lower wall up to a Reynolds number of 1000. A thorough review on this subject may be found in the works of Nie and Armaly [10], Chiang and Sheu [11] as well as Williams and Baker [9]. Later works include those of Biswas *et al.* [12], Barbosa Saldana *et al.* [13], Kitoh *et al.* [14] and Nie *et al.* [15]. The issue of the secondary eddy along the upper wall has been addressed by Chiang and Sheu [11], Williams and Baker [9], Tylli *et al.* [6] and Kitoh *et al.* [14].

Chiang and Sheu [11] were able to predict the secondary eddy only for aspect ratios greater than the one used in the test section of Armaly *et al.* [3]. Williams and Baker [9, p. 1171] showed the development of the secondary eddy that is confined in a region close to the plane of symmetry and does not extend all the way to the lateral wall. Kitoh *et al.* [14, p. 1148] gave only qualitative characteristics of the secondary eddies along the upper wall, which are created at the lateral wall and may or may not extend all the way to the plane of symmetry depending on the expansion ratio of the step. Tilly *et al.* [6, p. 3840] also computed this secondary eddy, which is located close to the lateral wall and does not penetrate to the plane of symmetry. Biswas *et al.* [12, p. 371] also came to similar conclusions as Kitoh *et al.* [14] and Tilly *et al.* [6] regarding the eddy along the upper wall.

All of these authors reported a very good agreement of their calculations with the data of Armaly *et al.* [3] or with other two-dimensional computations for the reattachment length of the eddy along the lower wall. There is a complete lack of report of numerical data of these authors regarding the secondary eddy and a consequent comparison with available experimental data by Armaly *et al.* [3] or by Lee and Mateescu [5] or with the numerous two-dimensional computations on that subject (e.g., Erturk [7]). Surprisingly, almost none of the authors who even performed two-dimensional computations have compared their predictions with the available experimental data for the secondary eddy with the exception of Lee and Mateescu [5, p. 714], Romé *et al.* [16, p. 1261], and Barton [17].

This work intends to alleviate the shortcomings of previous three-dimensional computations in the laminar flow over a backward-facing step by presenting results in a computational domain that uses the geometry of the test section of the experiments of Armaly *et al.* [3]. Two computational codes are used in order to enhance the credibility of the predictions: FEFLO and FEM3D.

In the following, the governing equations are given along with the appropriate boundary conditions. The numerical methods and codes used are then briefly presented. Finally, the results are discussed in detail and conclusions drawn.

2. DOMAIN CONSIDERED, GOVERNING EQUATIONS, AND BOUNDARY CONDITIONS

The computational domain for the laminar three-dimensional flow over a backward-facing step considered here is shown in Figure 1. The streamwise, transverse, and spanwise directions are aligned with the x, y, and z axes, respectively. A cross section of the domain perpendicular to the spanwise direction is also shown in the same figure.

DOI: 10.1002/fld

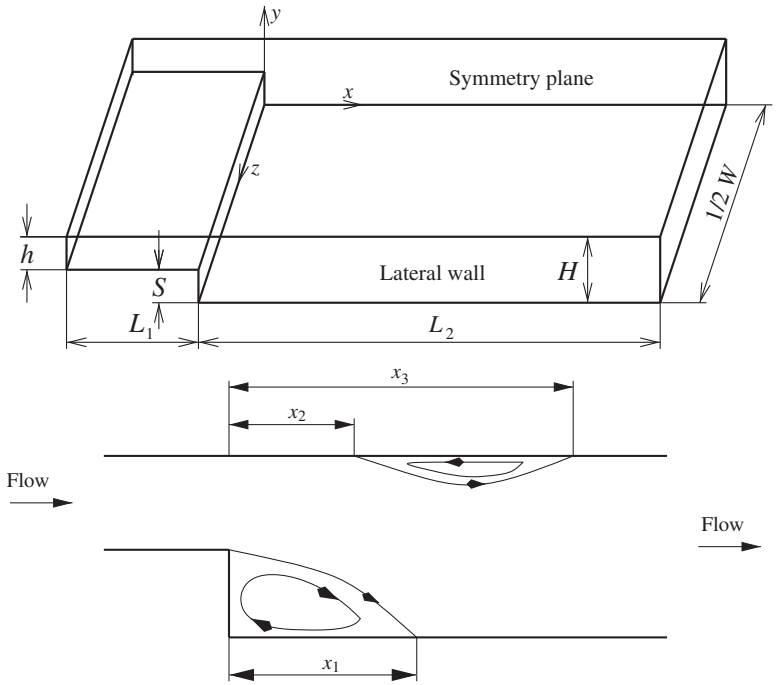

Figure 1. A sketch of the computational domain of this work.

An incompressible Newtonian fluid of constant viscosity and density enters the computational domain and flows all the way up to the exit. The computational domain is a combination of two cuboids, which are a small channel and a big channel with heights of $h = 5.2$ mm and $H = 10.1$ mm, respectively. The small channel is mounted upstream of the entrance of the big channel at the step of the domain. The height of the step is $S = 4.9$ mm. These are the same dimensions of the test section where Armaly *et al.* [3] conducted their laboratory experiments. The expansion ratio of the domain is $h{:}H = 1{:}1.94$. The aspect ratio of the domain is $S{:}W = 1{:}36.7$. In Figure 1, only half of the domain is considered in the spanwise direction, as the flow is expected to be symmetric with respect to the plane of symmetry. Actually, it has been reported by Armaly *et al.* [3, p. 474] that the flow maintained symmetry with respect to the centerplane of their test section for the whole range of Reynolds numbers studied.

Two eddies are sketched in the two-dimensional cross section of the domain in Figure 1. Because of the expansion of the flow over the step, an eddy is formed along the lower wall of the channel downstream of the step. The reattachment length of this eddy is x_1. When the Reynolds number is greater than 400, a second eddy is formed along the upper wall. This eddy has been first reported by Armay *et al.* [3] and has been later confirmed by many two-dimensional computations (e.g., Kim and Moin [18], Gartling [19], Erturk [7] and references therein). The detachment position of this eddy is x_2, and its reattachment position is x_3. The numerical data for positions x_1, x_2, and x_3 are usually given for comparisons among the authors who have performed computations and laboratory experiments over the course of the years. The values for these positions are the main results of this work as well.

The Navier–Stokes equations describing isothermal flow of an incompressible Newtonian fluid are given in a nondimensional form by

$$\nabla \cdot \mathbf{u} = 0 \tag{1}$$

$$\mathbf{u}_{,t} + \mathbf{u} \cdot \nabla \mathbf{u} = -\nabla p + \frac{1}{Re} \nabla \cdot \{\nabla \mathbf{u} + (\nabla \mathbf{u})^T\}. \tag{2}$$

Here, $\mathbf{u} = (u, v, w)$ is the dimensionless velocity vector in the fluid, with u, v, w as its components in the x, y, z directions, respectively. The governing equations have been rendered dimensionless

DOI: 10.1002/fld

by choosing the height H of the channel downstream of the step as the characteristic length and the average velocity U in the channel with height H as the characteristic velocity. Here, p is the dimensionless pressure, $Re = \rho UH/\mu$ the Reynolds number with ρ as the density, and μ the dynamic viscosity of the fluid. This definition of the Reynolds number has a consequence that the magnitude of Re in this work is half the one calculated from the more conventional definition found in the work of Armaly *et al.* [3] and followed by most authors who performed computations. This difference in the two definitions of the Reynolds number has also been pointed out by Chiang and Sheu [11, p. 863] who used the height of the inlet channel h and the average velocity in this channel as the characteristic length and velocity, respectively. However, the results in Section 4 are presented with the more conventional definition of the Reynolds number introduced by Armaly *et al.* [3]. The pressure p has been nondimensionalized with the magnitude ρU^2.

The boundary conditions for this flow are as follows:

At the entrance ($x = -4, 0 \leqslant y \leqslant 1, 0 \leqslant z < W/2H$):

$$u = \frac{6}{\left(\frac{h}{H}\right)^3}\left[y^2 + \left(\frac{h}{H} - 2\right)y - \left(\frac{h}{H} - 1\right)\right] \tag{3}$$

$$v = 0 \tag{4}$$

$$w = 0 \tag{5}$$

Along the walls of the domain and the step:

$$u = 0 \tag{6}$$

$$v = 0 \tag{7}$$

$$w = 0 \tag{8}$$

Along the plane of symmetry:

$$w = 0 \tag{9}$$

$$\frac{\partial u}{\partial z} = 0 \tag{10}$$

$$\frac{\partial v}{\partial z} = 0 \tag{11}$$

At the outflow: free boundary condition

Equations (3)–(5) impose a parabolic slit flow at the entrance of the computational domain. It should be noted that the entrance of the domain L_1 is located four units of length H upstream of the step (Figure 1). It is stated in the literature (Erturk [7, p. 646] and references therein; Schäfer *et al.* [1, p. 91]) that five units of length h are sufficient to assume a fully laminar, parabolic, one-dimensional profile for the streamwise velocity at the entrance. Our choice lies on the safer side of this assumption ($5h < 4H = 7.7h$).

The no-slip boundary condition (Equations (6)–(8)) has been imposed along the horizontal walls of the domain as well as along the step and the lateral wall. By applying the no-slip boundary condition along the lateral wall, a thorough study of the flow phenomena is enabled in the proximity of that region, as will be discussed in Sections 4.5 and 4.6. The symmetry boundary condition (Equations (9)–(10)) is imposed along the plane of symmetry.

For FEM3D, the free boundary condition has been applied at the outflow, in order to let the fluid leave the computational domain freely without any distortion of the flow in the interior. This outflow boundary condition has been first applied to the laminar flow over a two-dimensional backward-facing step by Papanastasiou *et al.* [20]. Ever since, this concept has found a wide use (e.g., Zienkiewicz and Taylor [21, vol. 3, p. 82]; Colonius [22, p. 333]; Sayag and Tziperman [23, p. 492]). For a numerical formulation of the free boundary condition, the reader is referred to the discussion of Equation (14). For FEFLO, the pressure is imposed at the outflow.

DOI: 10.1002/fld

In connection with the outflow boundary condition, it should be noted that the choice of the length of the computational domain L_2 is a complicated issue because the outflow is artificial (Figure 1). It is outside the scope of this work to get into any further details regarding artificial outflows and appropriate boundary conditions. What matters here is to choose the outflow sufficiently away from the step and the reattachment position of the eddy along the upper wall, so that the phenomena of separation are not going to be affected in any way. The experience with this flow shows that the reattachment length of the eddy along the upper wall of the domain is about 10 units of length H (e.g., Armaly *et al.* [3]; Gartling [19]) at $Re = 800$. In this work, a choice of 20 units of length H downstream of the step guarantees that the flow phenomena to be studied are going to be unaffected independent of the choice of the outflow boundary condition.

3. FINITE ELEMENT FORMULATION AND CODES USED

The computational results of this work have been obtained with two different codes: FEM3D and FEFLO. In this section, both codes are briefly discussed in connection with the finite element formulation of the Navier–Stokes equations.

3.1. FEM3D

FEM3D uses P2/P1 hexahedral elements, that is, each cuboid has 27 velocity nodes and eight pressure nodes. The coordinates of the vertices of each cuboid for the computational domain of this work are given in Table I. The mesh for the data of Table I is shown in Figure 2.

A standard Galerkin finite element formulation (e.g., Zienkiewicz and Taylor [21], Gresho and Sani [24], Owen and Hinton [25]) is used. Velocities and pressure are approximated with Lagrangian triquadratic ϕ^i and trilinear ψ^i basis functions in each element as follows:

$$u = \sum_{i=1}^{27} u_i \phi^i, v = \sum_{i=1}^{27} v_i \phi^i, w = \sum_{i=1}^{27} u_i \phi^i, p = \sum_{i=1}^{8} p_i \psi^i.$$

Table I. Computational details of code FEM3D.

Total number of elements									102,180
Elements in x-direction, before the step									32
Elements in x-direction, after the step									115
Elements in y-direction									20
Elements in z-direction									39
Number of nodes									854,385
Number of unknowns									2,484,858
Maximum front width									10,220
x-coordinates of the vertices									
−4.0000	−3.75	−3.50	−3.25	−2.75000	−2.500000	−2.0000000	−1.75000	−1.5000	−1.2500
−1.0000	−0.95	−0.90	−0.85	−0.80000	−0.750000	−0.7000000	−0.65000	−0.6000	−0.5500
0.0500	0.10	0.15	0.20	0.25000	0.300000	0.3500000	0.40000	0.4500	0.5000
0.5500	0.60	0.70	0.75	0.80000	0.850000	0.9000000	0.95000	1.0000	1.2000
1.4000	1.60	1.80	2.00	2.20000	2.400000	2.6000000	2.80000	3.0000	3.2000
3.4000	3.60	3.80	4.00	...	20.000000				
y-coordinates of the vertices									
0.0000	0.05	0.10	0.15	0.20000	0.250000	0.3000000	0.35000	0.4000	0.4500
0.4851	0.55	0.60	0.65	0.70000	0.750000	0.8000000	0.85000	0.9000	0.9500
1.0000									
z-coordinates of the vertices									
0.0000	0.25	0.50	0.75	1.00000	1.500000	2.0000000	2.50000	3.0000	3.5000
4.0000	4.50	5.00	5.50	6.00000	6.500000	7.0000000	7.20000	7.4000	7.6000
7.8000	8.00	8.10	8.20	8.30000	8.400000	8.5000000	8.60000	8.7000	8.8000
8.8200	8.84	8.86	8.88	8.89545	8.903175	8.9070375	8.90896	8.9099	8.9109

DOI: 10.1002/fld

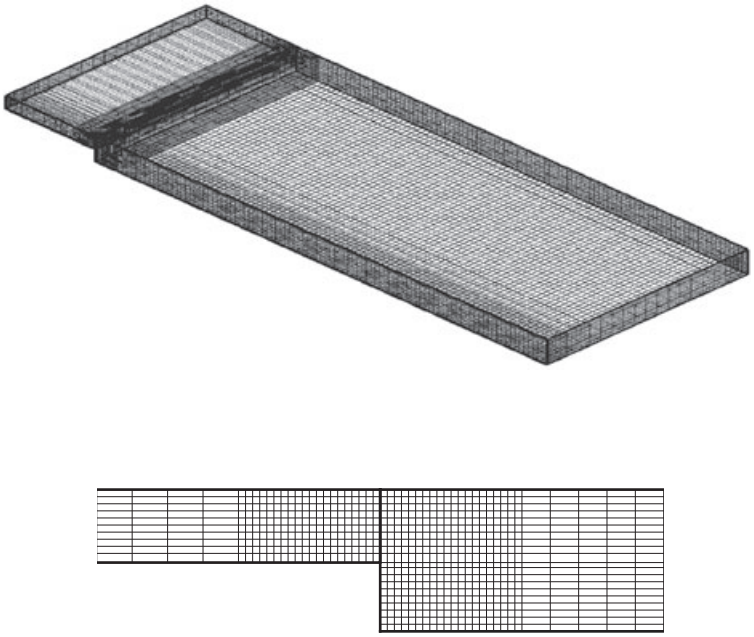

Figure 2. The mesh in three dimensions along with a two-dimensional view of any plane perpendicular to the z-axis in the region $2 \leqslant x \leqslant 2$.

These approximations are inserted into Equations (1) and (2), which are weighted integrally with basis functions ψ^i and ϕ^i, respectively, in order to obtain the following continuity, R_C^i, and momentum, R_M^i, residuals:

$$R_C^i = \int_V \nabla \cdot \mathbf{u}\, \psi^i \, \mathrm{d}V \tag{12}$$

$$R_M^i = \int_V \left[\mathbf{u} \cdot \nabla \mathbf{u} - \nabla \cdot \left(-p\, \mathbf{I} + \frac{1}{Re} \{ \nabla \mathbf{u} + (\nabla \mathbf{u})^T \} \right) \right] \phi^i \, \mathrm{d}V. \tag{13}$$

By applying the divergence theorem, in order to decrease the order of differentiation and to project possible natural (Neumann type) boundary conditions, we can reduce Equation (13) to

$$R_M^i = \int_V \left[\mathbf{u} \cdot \nabla \mathbf{u}\, \phi^i - \left(-p\, \mathbf{I} + \frac{1}{Re} \{ \nabla \mathbf{u} + (\nabla \mathbf{u})^T \} \right) \cdot \nabla \phi^i \right] \mathrm{d}V - \int_S \mathbf{n} \cdot \left[-p\, \mathbf{I} + \frac{1}{Re} \{ \nabla \mathbf{u} + (\nabla \mathbf{u})^T \} \right] \phi^i \, \mathrm{d}S. \tag{14}$$

The residuals of the continuity Equation (12) are evaluated at all vertices of the computational domain. The volume integral of the momentum residual (14) is evaluated at all nodes of the computational domain (vertices plus midnodes) unless it is replaced by essential boundary conditions, as discussed in the succeeding paragraphs. The surface integral of Equation (14) is evaluated only along the boundary surfaces of the computational domain. Because of the fact that essential boundary conditions are valid along all but the symmetry plane as well as the outflow of the domain, Equation (14) is going to be replaced by Equations (3)–(8). Along the plane of symmetry, both natural (Equations (10) and (11)) and essential (Equation (9)) boundary conditions apply. This means that the surface integrals of the residuals of Equation (14), which correspond to the u-velocity and the v-velocity, become zero. The momentum residual of Equation (14), which corresponds to the w-velocity, is replaced with Equation (9). Finally, the surface integral of Equation (14) is evaluated along the outflow of the domain because no assumption has been made regarding the development of the flow. The calculation of the surface integral along the outflow of the domain is the imposition of the free boundary condition.

DOI: 10.1002/fld

Equations (12) and (14) along with the essential boundary conditions (3)–(9) represent a nonlinear system of algebraic equations. This is solved using a Newton–Raphson iterative scheme. The convergence criterion imposed was $1{\cdot}10^{-7}$ for the velocities and $1{\cdot}10^{-4}$ for the pressure. Gaussian elimination (i.e., a direct solver) is used for the inversion of the Jacobian matrix, which is formed by analytically differentiating the residuals R_C^i and R_M^i with respect to the nodal unknowns u^i, v^i, w^i, and p^i.

The finite element code was written in FORTRAN 90. The solution of the linearized system of equations with Gaussian elimination is the most time-consuming step in the execution of the computational code. A parallel direct solver has been written for this purpose. It is based on the serial frontal solver introduced by Irons [26] and later extended by Hood [27] and has been ported to a distributed parallel computing environment.

The production runs have been performed on the SGI ICE machine (Sunnyvale, CA, USA) at the George Mason University. The machine is composed of 640 Intel processors (Santa Clara, CA, USA) running at 2.3 GHz. Each node contains two processors, and the nodes are grouped into 80 blades or nodes of eight cores each node (two quad-core Xeon processors Harpertown E5440 series, Intel). It reaches a peak performance of 6 TFLOPS. The main memory has a capacity of 1.25 TB. Disk storage capacity is 28 TB, and scratch disk capacity exceeds 36 TB. The interconnection network is composed of two InfiniBand interconnects (10/20 Gb/s); one interconnect is dedicated to I/O and the other to MPI traffic. The operating system is the Suse Linux Enterprise 10 (Novell, Waltham, MA, USA) tuned for SGI.

The current performance of FEM3D is such that using 256 cores for 24 h is needed for successful convergence at each Reynolds number with the problem size of Table I. Preliminary runs have also been performed on a Cray XT5 system (Seattle, WA, USA; Kraken, located at Oak Ridge National Laboratory) and BlueGene (IBM, Armonk, NY, USA; located at NCAR).

Two-dimensional computations have also been made with FEM3D by using one element in the z-direction. In this way, the deviation of the three-dimensional results from the expected values obtained from two-dimensional numerical experiments may be evaluated on a fair basis, where the only difference is going to be the dimensionality of the flow and everything else is the same.

3.2. FEFLO

FEFLO was conceived as a general-purpose computation fluid dynamics code based on the following principles:

- Use of unstructured grids (automatic grid generation and mesh refinement);
- Finite element discretization of space;
- Separate flow modules for compressible and incompressible flows;
- Arbitrary Lagrangian–Eulerian formulation for moving grids;
- Edge-based data structures for speed and the use of limiting and upwinding;
- Optimal data structures for different architectures;
- Bottom-up coding from the subroutine level to assure an open-ended, expandable architecture.

The code has been ported to vector, shared-memory parallel (via OMP [28]) and distributed-memory parallel (via MPI [29]), machines. The usual difficulties associated with the first-order operators are treated via limiting and upwinding for the advection operator [30] and fourth-order damping for the divergence constraint [31, 32]. The equations are advanced in time by using the following projection-type solver:

(a) Advective–diffusive prediction: $\mathbf{v}^n \rightarrow \mathbf{v}^*$

$$\left[\frac{1}{\Delta t} + \mathbf{v}^n \cdot \nabla - \nabla \mu \nabla\right](\mathbf{v}^* - \mathbf{v}^n) + \mathbf{v}^n \cdot \nabla \mathbf{v}^n + \nabla p^n = \nabla \mu \nabla \mathbf{v}^n; \tag{15}$$

(b) Pressure correction: $p^n \rightarrow p^{n+1}$

$$\nabla \cdot \mathbf{v}^{n+1} = 0; \tag{16}$$

DOI: 10.1002/fld

$$\frac{\mathbf{v}^{n+1} - \mathbf{v}^*}{\Delta t} + \nabla(p^{n+1} - p^n) = 0; \tag{17}$$

which results in

$$\nabla^2(p^{n+1} - p^n) = \frac{\nabla \cdot \mathbf{v}^*}{\Delta t} \tag{18}$$

(c) Velocity correction: $\mathbf{v}^* \rightarrow \mathbf{v}^{n+1}$

$$\mathbf{v}^{n+1} = \mathbf{v}^* - \Delta t \nabla(p^{n+1} - p^n). \tag{19}$$

The solution is advanced in time by using local time steps with a Courant number of $Cou = 5$, until steady state is reached. Note that at steady state, the residuals of the pressure correction vanish, which implies that the result does not depend on the time step Δt. The implicit advection system is advanced using an lower–upper symmetric Gauss–Seidel relaxation. The pressure equation is solved using linelet [33] and diagonally preconditioned conjugate gradient algorithms with projective pressure prediction [34].

For FEFLO, the mesh shown in Figure 3 was used. The total number of elements and points was 23.13 million tetrahedra and 3.98 million points, respectively, and the distance from the wall for the first element was $h_n = 0.9 \cdot 10^{-3}$. The current performance of FEFLO is such that using one processor for 24 h is needed for successful convergence at each Reynolds number with the mesh shown in Figure 3.

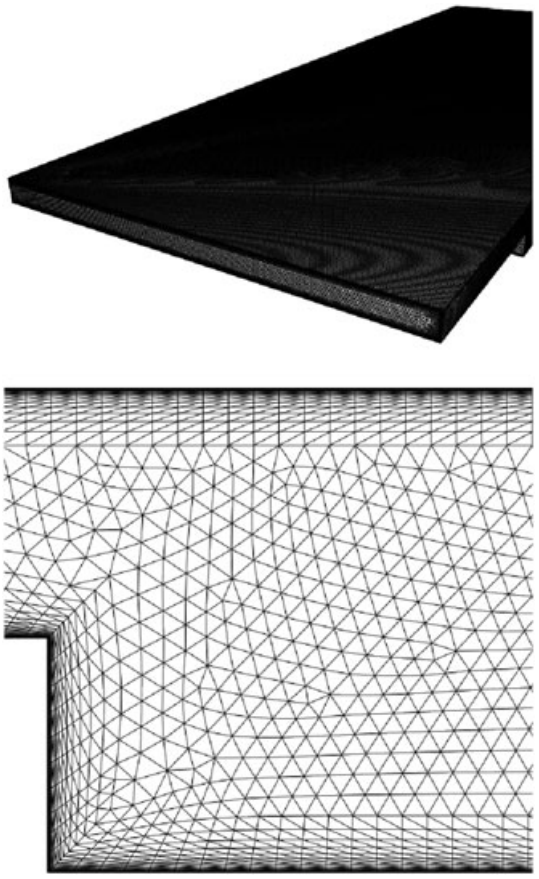

Figure 3. The three-dimensional unstructured mesh used in FEFLO along with a detailed look in any plane perpendicular to the z-axis.

DOI: 10.1002/fld

4. RESULTS AND DISCUSSION

The results of this work are the three-dimensional computations of FEM3D and FEFLO with the use of the methodology described in the previous section and the two-dimensional computations of FEM3D. The three-dimensional results are compared for their deviation from the two-dimensional results. In addition, the three-dimensional results are compared with the available laboratory experiments performed by Armaly *et al.* [3], which have been obtained using a test section with the same geometry as Figure 1. Additional comparisons have been made with the laboratory data of Lee and Mateescu [5] who used a test section with a similar geometry as Figure 1.

Finally, the validity of the two-dimensional computations of this work is compared with the available numerical experiments by Erturk [7], in order to support the reliability of the computations of this work and the credibility of the conclusions. This is the first time that three-dimensional computations are scrutinized for their accuracy from all possible sources.

All three-dimensional computations are reported at the plane of symmetry as is the case with the laboratory experimental results. Because the results of the laboratory experimental data were reported in graphs, these graphs have been optically scanned and interpolated to produce the relevant cited quantities. In the following sections, the three-dimensional results of the code FEM3D are used for the comparison with the two-dimensional computations because the same code produced the two-dimensional results as well. A brief comparison of the codes FEM3D and FEFLO is made at the end of Section 4.4.

4.1. Validity of the two-dimensional calculations of this work

The two-dimensional computations of FEM3D are compared with available numerical results in the literature in order to enhance the reliability of the conclusions. A recent work by Erturk [7] represents the most comprehensive numerical study of the two-dimensional backward-facing step at steady state. Among the many cases that this author computed was also the geometry of the symmetry plane of Figure 1. Our computations are compared with Erturk's in Tables II–IV. The highest deviation of the results of this work from those of Erturk's are observed in the computation of the detachment position x_2 at $Re = 1000$ (8.5%) (Figure 1). For the rest of the Reynolds numbers, the deviation is of the order of 7.5%. Regarding the reattachment positions x_1 and x_3, the highest deviations are 2.2% and 3.4%, respectively, at $Re = 1000$.

It should be noted that the deviation is computed as $|x - y| / H$ with x the value of Erturk's work, y the value of this work, and H the height of the big channel as shown in Figure 1. It is concluded that the two-dimensional results of this work may be regarded as accurate. They are the basis for the comparison with the three-dimensional results. That is, the deviation of all three-dimensional results that are reported in the next section is calculated as $|x - y| / H$ with x the three-dimensional value and y the two-dimensional value of this work.

Table II. Reattachment length x_1, lower wall.

Re	3D computations FEM3D/FEFLO	2D computations FEM3D	2D computations Erturk [7]	Lee and Mateescu experiment [5]/ Armaly *et al.* experiment [3]
100	1.3923/1.36	1.3919	1.3963	—/1.41
200	2.3727/2.35	2.3759	2.3772	—/2.29
300	3.2321/—	3.2311	3.2306	—/3.11
400	3.9971/3.87	3.9707	3.9675	—/4.03
500	4.6551/—	4.5809	4.5783	4.51/4.86
600	5.1981/4.66	5.0637	5.0669	5.09/5.49
648	5.4133/5.24	5.2689	—	5.36/6.07
700	5.6163/—	5.4569	5.4652	5.49/6.25
800	5.9331/5.70	5.8018	5.8135	6.32/6.94
900	6.1893/—	6.1165	6.1337	6.67/7.64
1000	6.4271/6.07	6.4143	6.4365	7.49/8.06
1050	6.5547/—	6.5611		7.71/8.54

DOI: 10.1002/fld

Table III. Detachment position x_2, upper wall.

Re	3D computations FEM3D/FEFLO	2D computations FEM3D	2D computations Erturk [7]	Lee and Mateescu experiment [5]/ Armaly *et al.* experiment [3]
500	4.1643/—	3.9561	4.0335	3.75/4.17
600	4.3652/4.09	4.1594	4.2315	4.24/4.58
648	4.4699/4.39	4.2695	—	4.51/4.86
700	4.5745/—	4.3801	4.4537	4.58/4.99
800	4.7477/4.60	4.6043	4.6797	5.21/5.56
900	4.9017/—	4.8289	4.9092	5.56/6.32
1000	5.0691/4.86	5.0533	5.1387	6.42/6.84
1050	5.1657/—	5.1655		6.67/7.29

It should also be noted that the two-dimensional computations of FEM3D are mesh independent. When the elements in both the x-direction and y-direction are doubled, the numerical results do not change in the first two decimal points.

An interesting issue with the two-dimensional computations for this flow is that all authors who performed computations in the range $100 \leqslant Re \leqslant 800$ observed a steady increase in the reattachment length x_1 of the eddy along the lower wall. This phenomenon has also been reported by Armaly *et al.* [3]. However, the computations of all authors starting with Osswald *et al.* [35, p. 694], Kim and Moin [18, p. 321], Kaiktsis *et al.* [36, p. 503] until Erturk [7, p. 641] show a change in the slope of x_1 with respect to the Reynolds number for $Re > 400$. The consequence is that the reattachment length x_1 is systematically underpredicted with respect to the experimental measurements for calculations at $Re > 400$. Indeed, the measurements by Armaly *et al.* [3] show a steady increase of x_1 with respect to Re without any appreciable change in the slope up to $Re = 1200$. This observation has been further confirmed in the experiments of Lee and Mattescu [5, p. 711], although they report two-dimensional results without three-dimensional effects.

Intuitively, one expects a change in the slope at $Re = 400$ because a second eddy appears along the upper wall, which hinders the development of the eddy along the lower wall. All two-dimensional calculations account for this phenomenon. A very comprehensive discussion on that issue has been performed by Tylli *et al.* [6, p. 3840] and Williams and Baker [9, p. 1172]. Because of the fact that Armaly *et al.* [3] have reported three-dimensional effects in their experiments for $Re > 400$, this issue of change of slope has remained unresolved so far. In the next subsection, we address this discrepancy once again with the additional information from three-dimensional computations that predict the eddy along the upper wall (Figure 4).

4.2. The reattachment length of the eddy along the lower wall

The computations of the reattachment length x_1 of the eddy along the lower wall are given in Table II along with the data of other authors for comparison. It is a well-known fact in the literature that the flow for $Re \leqslant 400$ is two-dimensional for the expansion ratio of Figure 1. This fact has been established by Armaly *et al.* [3]; it has been verified by two-dimensional calculations of the same authors in the same paper, and it has been undisputed ever since. The results of this work verify once again this fact. The deviation of the three-dimensional results is less than 2.6% with respect to the two-dimensional computations of this work. The corresponding measurements by Armaly *et al.* [3] also deviate less than 12.1% with respect to the calculations for $Re \leqslant 400$.

The deviation of the three-dimensional computations from the two-dimensional ones increases from 7.4% at $Re = 500$ to a maximum of 15.9% at $Re = 700$ and then monotonically decreases up to 0.6% at $Re = 1050$. That is, the three-dimensional computations may be called two-dimensional along the plane of symmetry for the computational domain of Figure 1. This is the first time that three-dimensional computations are reported to be so close to two-dimensional calculations.

It should be noted, though, that the results of the code have been obtained in the following way. A solution at a very low Reynolds number was computed first ($Re = 0.02$); this solution was used as an initial guess for a higher Reynolds number and so on (zero-order continuation). At each Reynolds

DOI: 10.1002/fld

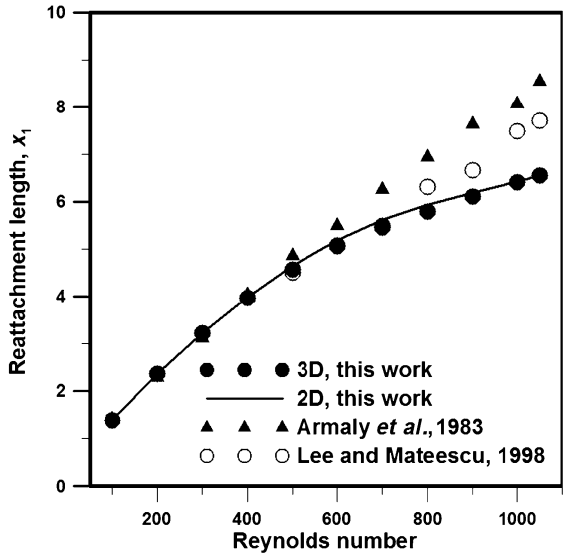

Figure 4. Comparison of two-dimensional and three-dimensional computations of this work along with experimental data and demonstration of the blockage effect in the geometry of Armaly *et al.* [3].

number, five iterations were necessary for successful convergence of the code without observing any anomaly in the sequence of the iterations. The computational results were also mesh independent. When the number of elements in the z-direction are doubled, the results did not change in the first two decimal points along the plane of symmetry. This behavior of the code leads to the conclusion that the computational results are reliable in the whole range of Reynolds number studied.

The deviation of the experimental measurements by Armaly *et al.* [3] with respect to the two-dimensional computations starts at 27.9% ($Re = 500$) and increases monotonically to 198% ($Re = 1050$). The situation is somehow different for the experimental data of Lee and Mateescu [5]. The deviation is negligible for $Re \leqslant 700$ (less than 9%), grows to 55% for $800 \leqslant Re \leqslant 900$, and goes to almost 115% for $1000 \leqslant Re \leqslant 1050$. The results of Lee and Mateescu [5] have been obtained with an aspect ratio of 1:40 and an expansion ratio of 1:2. The difference in the expansion ratio between the two experimental test sections should be negligible, as pointed out in the calculations by Erturk [7, p. 652]. However, the aspect ratio of Lee and Mateescu [5] is bigger than that of Armaly *et al.* [3], so that it is expected that their results are closer to the two-dimensional calculations.

A deviation in the reattachment length of up to one unit of height between three-dimensional measurements and two-dimensional computations may be regarded as acceptable from an engineering point of view, in order to consider the data by Lee and Mateescu [5] as two-dimensional. After all, they call their experiments two-dimensional, although they avoid a comparison between two-dimensional and three-dimensional results in their work apart from one case at $Re = 800$ where a direct comparison of reattachment and detachment positions is made (p. 714 of their work). They support the two-dimensional nature of their experiments intuitively by choosing a relatively high aspect ratio (p. 705 of their work), and they present two-dimensional calculations of velocity profiles at $Re = 800$ (p. 709 of their work), which show a very good agreement between computations and data.

On the other hand, the situation with the measurements of Armaly *et al.* [3] is more complicated than that of Lee and Mateescu. A maximum deviation of two units of height is relatively high compared with the deviation of the measurements by Lee and Mateescu [5] to call the data two-dimensional. Armaly *et al.* [3] clearly made the point of three dimensionality in their experiments. They based their argumentation on the fact that spanwise velocity profiles at $Re > 400$ (p. 483 of their work) show a strong disturbance near the lateral wall, which is not the case for the corresponding spanwise velocity profiles at $Re < 400$ (p. 479 of their work). They also made two-dimensional

DOI: 10.1002/fld

computations that show no increase in the reattachment length for $Re > 500$ (pp. 488 and 490 of their work), which was used as an additional argument to support three dimensionality in the data.

In view, though, of the fact that our three-dimensional calculations are very close to the two-dimensional computations and that the two-dimensional computations of this work underpredict the data of Armaly *et al.* [3] by a margin of half a unit of height at $Re = 800$ and two units of height at $Re = 1050$, the three-dimensional character of their data should be reevaluated (Table II). After all, the data of Armaly *et al.* [3] are called two-dimensional in a later work by Nie and Armaly [10, pp. 4714 and 4717].

Finally, Figure 4 depicts the results of Table II. As discussed in the previous section, the blockage effect of the secondary eddy is evident in the length of the primary eddy in the three-dimensional calculations of this work because of the fact that the results deviate less than 16% from the two-dimensional computations. This is shown for the first time in the geometry of the experiment of Armaly *et al.* [3]. In the same figure, the data of Armaly *et al.* [3] are shown along with those of Lee and Mateescu [5].

The issue of three dimensionality of the experimental data of Armaly *et al.* [3] is further elucidated in the discussion of the results regarding the eddy along the upper wall downstream of the step.

4.3. The detachment position of the eddy along the upper wall

The computations of the detachment position x_2 of the eddy along the upper wall are given in Table III along with the data of other authors for comparison. This is the first time that three-dimensional computations are reported for the eddy along the upper wall for this flow and are compared with the work of other authors. The results of Table III are depicted in Figure 5.

The maximum deviation between the three-dimensional and two-dimensional computations is 20% at $500 \leqslant Re \leqslant 650$. The deviation decreases monotonically for higher Reynolds numbers up to 1.5% at $Re = 1000$. At $Re = 1050$, the results of both computations are almost identical. The three-dimensional computations are again very close to the two-dimensional ones as in the previous subsection.

The experiments of Armaly *et al.* [3] deviate from the two-dimensional computations by 21.4% at $Re = 500$. The deviation increases monotonically to 212.4% at $Re = 1050$. This result is consistent with the previous discussion regarding the reattachment length x_1. The experiments of Lee and Mateescu [5] deviate from the two-dimensional calculations by less than 25% at $500 \leqslant Re \leqslant 700$.

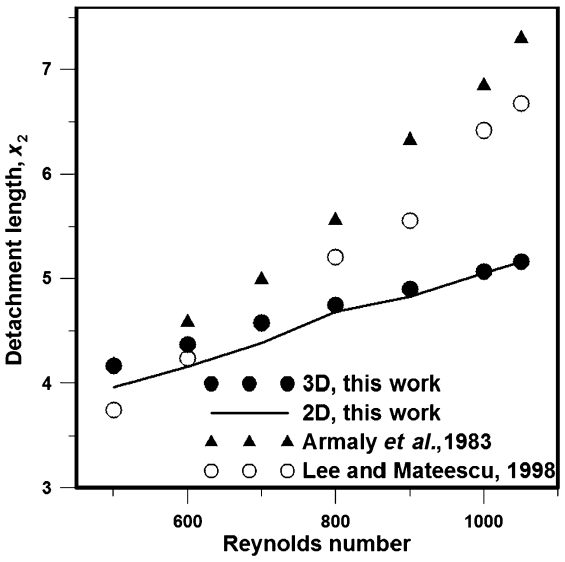

Figure 5. Comparison of two-dimensional and three-dimensional computations of this work along with the experimental data for the detachment position x_2 of the secondary eddy.

DOI: 10.1002/fld

The deviation then increases monotonically from 60.6% to 150% at $800 \leqslant Re \leqslant 1050$. This behavior is again consistent with the previous observations for x_1. However, the deviation of both experimental measurements from the two-dimensional calculations is higher in the case of the detachment position x_2 than in the case of the reattachment length x_1.

4.4. The reattachment position of the eddy along the upper wall

The computations of the reattachment position x_3 of the eddy along the upper wall are given in Table IV along with the data of other authors for comparison. The results of Table IV are depicted in Figure 6.

The highest deviation of the three-dimensional computations with respect to the two-dimensional ones is at $Re = 500$ (22.8%). The deviation decreases to 12.3% at $Re = 700$ and increases slightly up to 15.6% at $Re = 1050$. The results of the computations are very close to the two-dimensional calculations, as was the case for x_1 and x_2.

The experiments of Armaly *et al.* [3] show a deviation from the two-dimensional computations of between 19.4% and 42.1% in the region $500 \leqslant Re \leqslant 900$. The deviation increases up to 106.2% at $Re = 1050$. These results show a good agreement of the experimental measurements with the two-dimensional calculations. This is the first time that this fact has been observed because most authors have compared only the calculations of the reattachment length x_1. This observation sheds more light to a better understanding of the three-dimensional effects of the measurements by Armaly *et al.* [3]. In the case of the reattachment position x_3, the measurements may be regarded

Table IV. Reattachment position x_3, upper wall.

Re	3D computations FEM3D/FEFLO	2D computations FEM3D	2D computations Erturk [7]	Lee and Mateescu experiment [5]/ Armaly *et al.* experiment [3]
500	5.8657/—	6.0943	6.0663	6.79/5.90
600	7.2235/6.00	7.4164	7.3951	8.06/7.19
648	7.8239/7.39	8.0265	—	8.33/7.84
700	8.4881/—	8.6113	8.5886	8.47/8.19
800	9.5849/9.20	9.7257	9.6991	9.86/9.31
900	10.6593/—	10.7867	10.7562	10.42/10.42
1000	11.6797/10.38	11.8112	11.7770	11.12/10.90
1050	12.1547/—	12.3122	—	11.18/11.25

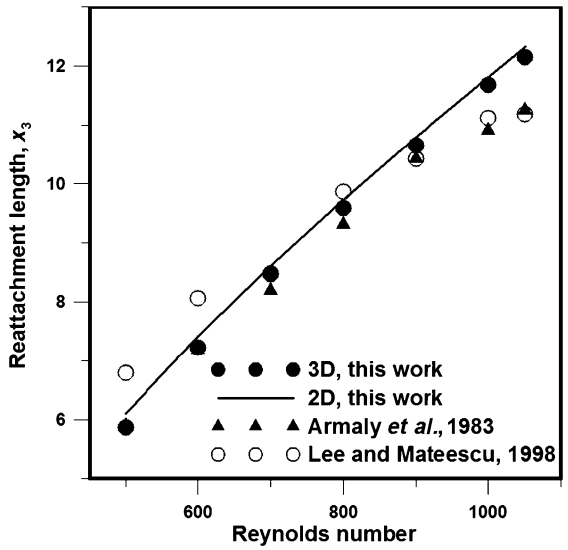

Figure 6. Comparison of two-dimensional and three-dimensional computations of this work along with experimental data for the reattachment position x_3 of the secondary eddy.

DOI: 10.1002/fld

as two-dimensional because of the relatively small deviation (up to one unit of height) from the two-dimensional calculations. In the experiments of Lee and Mateescu [5], the deviation from the two-dimensional calculations is between 13.4% and 113.2% in the range of $500 \leqslant Re \leqslant 1050$. The deviation drops from 69.5% to 13.4% at $500 \leqslant Re \leqslant 800$ and grows monotonically to 113.2% at $Re = 1050$. These measurements show less deviation than the corresponding ones for positions x_1 and x_2. This is also evident by inspecting Figures 4–6. This observation is carried out in this work for the first time.

A possible explanation of the closer agreement of the laboratory experiments with the two-dimensional calculations at position x_3 may be the fact that the flow phenomena at positions x_1 and x_2 are much more complicated than at position x_3 because one eddy reattaches and another one detaches. After all, positions x_1 and x_2 are very close to each other with x_2 preceding x_1 as calculated in this work and also observed by Armaly *et al.* [3, p. 480]. At position x_3, only one eddy reattaches, and the flow assumes a parabolic one-dimensional profile further downstream. This flow situation makes the measurements in the case of position x_3 by far simpler rather than in the case of positions x_1 and x_2. Although there is no doubt about the accuracy of the experiments and the methods used by both research groups, it is expected that, in case of deviations from two-dimensional results, the most vulnerable positions should be x_1 and x_2 rather than x_3.

It should be noted that x_2 and x_3 are closely related to each other because their difference is the length of the secondary eddy of the flow. These positions are measured separately in both the numerical and laboratory experiments. As the secondary eddy appears after a certain Reynolds number is reached, this phenomenon is associated with the detachment position x_2, which is critical in the evolution of this eddy. By studying the deviation of the detachment and the reattachment of the secondary eddy separately, one gets a complete picture of the flow in the whole domain, which may be hindered if only the deviation of the length of the secondary eddy would have been taken into account.

It should be also noted that the comparison of the three-dimensional results of the two codes shows in most cases a deviation of less than 40% between them at all Reynolds numbers apart from the reattachment length x_3 at $Re = 600$ and $Re = 1000$ where the deviation is one unit of height.

4.5. The effects of lateral walls

The effects of lateral walls are a very important issue in fluid mechanics both for numerical and laboratory experiments. De Brederode and Bradshaw [8] made a thorough study on this subject for laboratory experiments of separated flows, which is still followed in the literature [37, p. 105103-2]. It is beyond the scope of this work to even touch upon this issue. After all, there are two works in the literature [9, 11] that studied this issue extensively for the same geometry as in this work. Their results have been accepted as possible causes for the three-dimensional effects observed in the experiments of Armaly *et al.* [3] in a very recent paper by Schäfer *et al.* [1, p. 87].

However, the simple fact that the flow under consideration is expected to be distorted near the lateral wall and that it should attain gradually its two-dimensional configuration as it approaches the plane of symmetry should be kept in mind. In this work, we investigated this behavior of the flow by calculating streamlines along planes parallel and normal to the lateral wall. The results are depicted in Figures 7 and 8 for Reynolds numbers 800 and 400 because the streamlines for these Reynolds numbers are representative for the flow configurations with one (primary eddy at $Re \leqslant 400$) and two (both primary and secondary eddies at $Re > 400$) eddies.

It can be clearly observed from the figures that this expected phenomenon is indeed verified by our three-dimensional calculations. The streamlines shown in Figure 7 are reported for the first time because the codes of this work are capable of predicting both eddies. For both Reynolds numbers, the distortion of the flow is of the same nature close to the lateral wall as shown in Figures 7(a) and 8(a) in the sense that eddies are formed both along the lower and upper walls. However, as the flow develops away from the lateral wall, the two-dimensional characteristics of the flow are recovered completely, as has been discussed in the previous subsections. That is, the secondary eddy disappears at $Re = 400$ as the flow distances from the lateral wall. On the other hand, the secondary eddy is kept throughout the whole spanwise direction at $Re = 800$.

DOI: 10.1002/fld

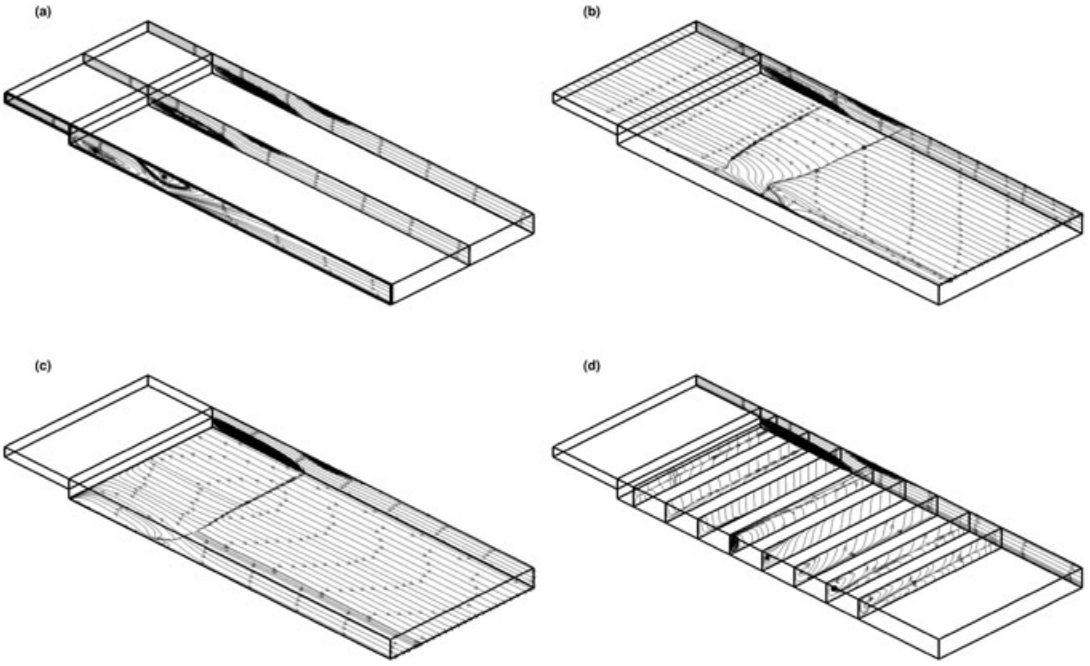

Figure 7. Computed streamlines at $Re = 800$. (a) In planes parallel to the lateral wall at spanwise locations $z = 8.8$, $z = 4$, and $z = 0$ (plane of symmetry); (b) in a plane normal to the lateral at location $y = 0.99$ along with the streamlines in the plane of symmetry; (c) in a plane normal to the lateral wall at location $y = 0.01$ along with the streamlines in the plane of symmetry; (d) in planes normal to the streamwise direction of the flow at locations $x = 1, 3, ..., 13$ along with the streamlines in the plane of symmetry.

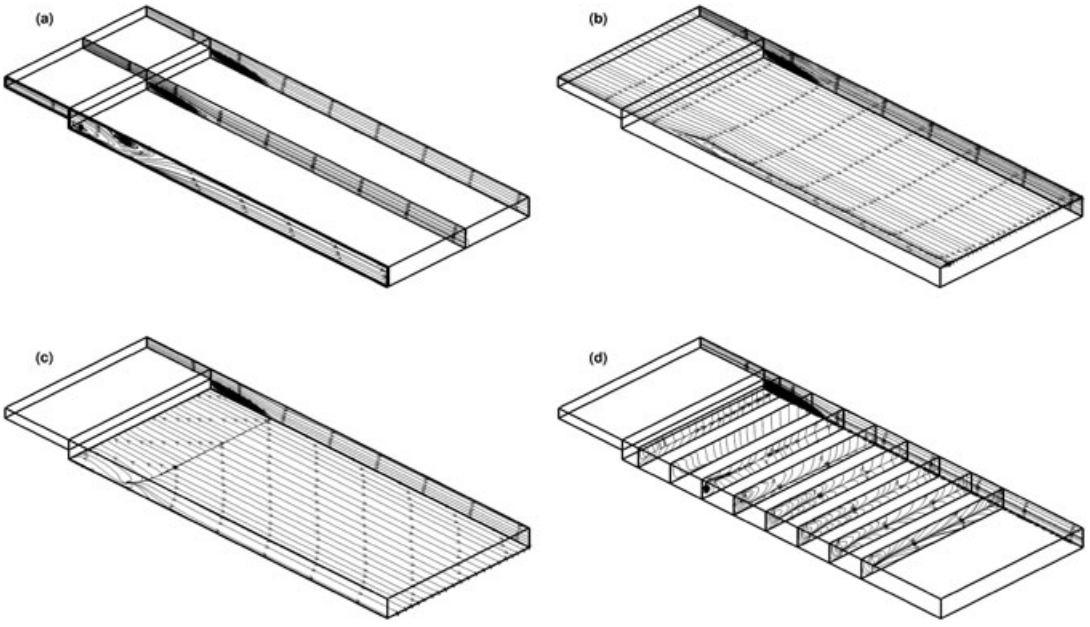

Figure 8. Computed streamlines at $Re = 400$. (a) In planes parallel to the lateral wall at spanwise locations $z = 8.8$, $z = 4$, and $z = 0$ (plane of symmetry); (b) in a plane normal to the lateral wall at location $y = 0.99$ along with the streamlines in the plane of symmetry; (c) in a plane normal to the lateral wall at location $y = 0.01$ along with the streamlines in the plane of symmetry; (d) in planes normal to the streamwise direction of the flow at locations $x = 1, 3, ..., 13$ along with the streamlines in the plane of symmetry.

DOI: 10.1002/fld

It should be noted that the high distortion of the flow near the lateral wall has been shown in the work of other authors (Chiang and Sheu [11, p. 182]; Williams and Baker 1997 [9, p. 1171]) as well. However, the use of a very fine mesh close to the lateral wall (as shown in Table I) along with the ability of the finite element method to perform well near boundaries with abrupt changes has enabled the penetration of the secondary eddy up to the plane of symmetry at $Re = 800$ and has obstructed the penetration of the secondary eddy in the plane of symmetry at $Re = 400$.

The distortion of the flow close to the lateral wall with respect to the formation or not of the secondary eddy may be studied deeper by observing the calculated streamlines in a plane normal to the transverse direction of the flow and close to the upper wall of the domain. This is shown in Figures 7(b) and 8(b). In Figure 7(b), it can be clearly seen that the limiting streamlines of the secondary eddy penetrate in the spanwise direction up to the point where the high distortion takes place close to the lateral wall. In Figure 8(b), there exists no secondary eddy, so that the high distortion near the lateral wall disappears in the interior of the domain because of the action of the streamlines that are parallel to the symmetry plane.

Limiting streamlines may also be observed in connection with the primary eddy of the flow as well. This is shown in Figures 7(c) and 8(c). In this case, the situation is completely analogous for both Reynolds numbers because the primary eddy exists in both cases. The limiting streamline of the primary eddy penetrates all the way up to the high distortion close to the lateral wall, as is the case with the limiting streamlines of the secondary eddy. This observation leads to the conclusion that there is no secondary flow associated with the eddy along the upper wall as was believed so far in the literature based on the calculations of Chiang and Sheu [11] and Williams and Baker [9].

Finally, computed streamlines are shown along planes perpendicular to the streamwise direction of the flow in Figures 7(d) and 8(d). These figures verify the existence of a secondary flow that has also been observed by Chiang and Sheu [11] and Williams and Baker [9]. This secondary flow is associated with the high distortion of the flow close to the lateral wall. It is confined up to a maximum of approximately two dimensionless units of lengths so that it affects by no means the flow phenomena in the plane of symmetry.

This behavior of the flow in three dimensions is verified once more in Figure 9. It is shown there how the streamwise velocity varies at position $y = 0.4851$ in the spanwise direction at five different streamwise locations ($1 \leqslant x \leqslant 5$) for the case of $Re = 800$. The value of the two-dimensional calculation for the same location is also plotted in the same figure for comparison. There are wall effects that cause a clear disturbance in the streamwise velocity. However, this disturbance fades

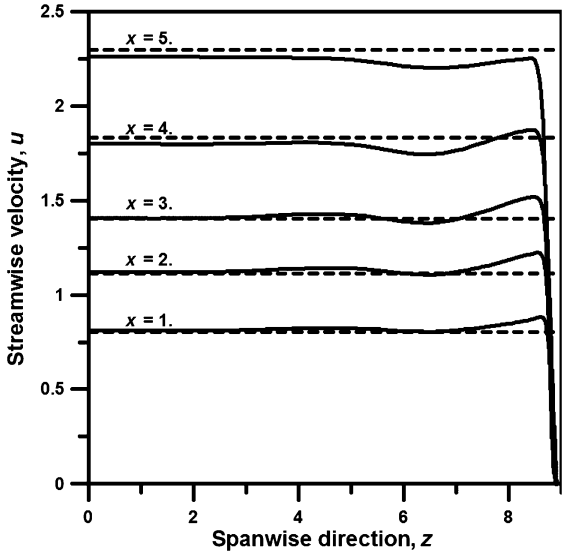

Figure 9. Computed spanwise values of the streamwise velocity at $y = 0.48$ at various streamwise locations. The corresponding two-dimensional values of the streamwise velocity are also given.

DOI: 10.1002/fld

away as the flow approaches the plane of symmetry. This figure is very representative for all cases of the flow studied in this work.

In addition, the variations of the length of the primary eddy at both Reynolds numbers are shown in Figure 10, along with the variation of the length of secondary eddy at $Re = 800$ as a function of the spanwise direction. The situation is analogous to the previous observations. There is a strong distortion of the magnitudes close to the wall, which decays as the flow approaches the plane of symmetry. The decay is faster for $Re = 400$ because the flow possesses only one eddy and the flow phenomena are less complex. However, the expansion ratio of 1:36.7 is adequate for higher Reynolds numbers to attain two-dimensional values as there seems to be enough room in the spanwise direction for the decay of the distortion according to the computations of this work.

The results in this figure show that the three-dimensional effects are unavoidable close to the lateral wall for both Reynolds numbers. In the original work of Armaly *et al.* [3], this issue has escaped their attention. They show results for $Re < 400$ up to $z = 8$ (figures 8 and 9 of their work), where any three-dimensional disturbance has disappeared, as is the case with Figure 10. They show three-dimensional effects for higher Reynolds numbers by taking measurements closer to the lateral wall where the variations are appreciable as in Figure 10. However, the numerical experiments of this work show that the three-dimensional effects are an issue close to the wall even at $Re = 400$. This issue is further elaborated in the next subsection.

4.6. Spanwise velocity profiles

In order to further elucidate the influence of the lateral wall, spanwise variations of the streamwise velocity u are shown in Figures 11–13 for two different Reynolds numbers. Results of both computational codes are compared with the data of Armaly *et al.* [3] and the two-dimensional predictions of FEM3D.

In Figure 11, the results at $Re = 397$ are depicted. The agreement of the numerical experiments with the laboratory data is relatively good (deviation of less than 8.1% with respect to the results of FEM3D) for cases in Figure 11(a)–(d). There is a much higher deviation for the case in Figure 11(c) with the experimental data. In Figures 12 and 13, the results at $Re = 648$ are depicted. The agreement between the computations and the experimental data is very good in most cases apart from the case in Figure 13(c).

There is, though, a common behavior of the three-dimensional computations of both codes close to the wall—irrespective of the difference of the codes in the value in the plane of symmetry—which

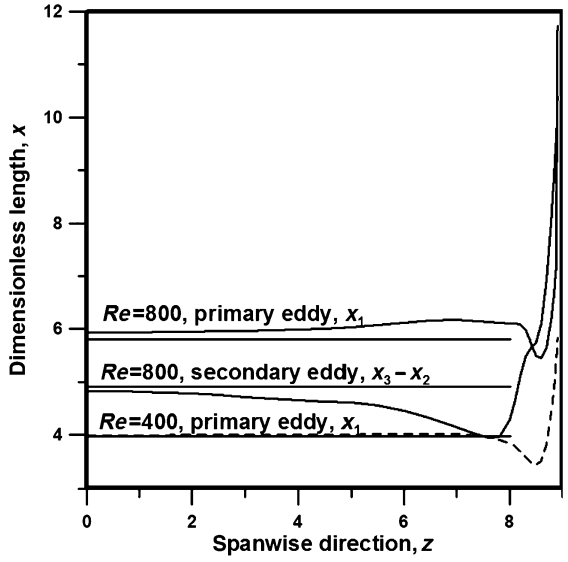

Figure 10. Spanwise variation of the lengths of the primary eddies at $Re = 400, 800$ and of the secondary eddy at $Re = 800$. The corresponding two-dimensional values of the lengths are also given.

DOI: 10.1002/fld

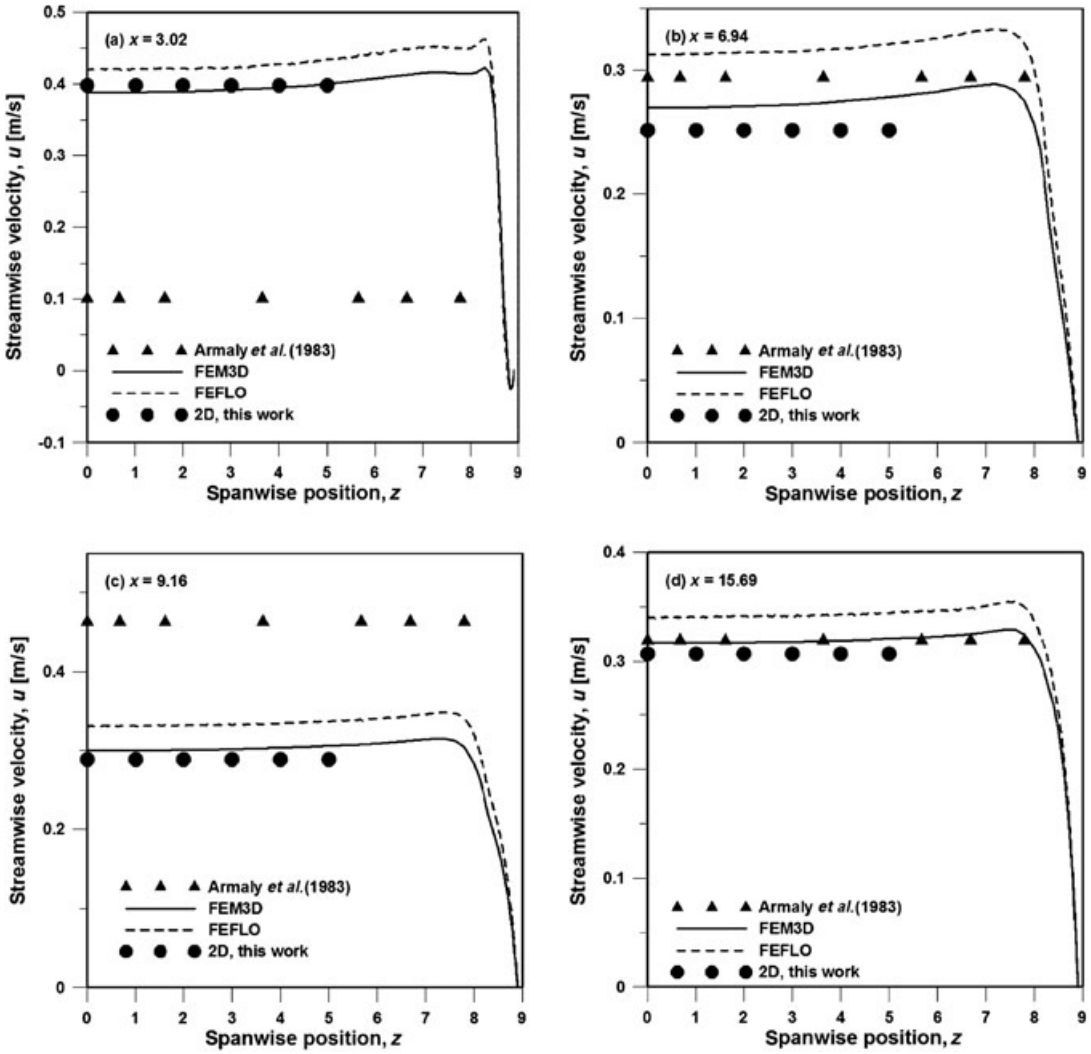

Figure 11. (a)–(d) Variation of streamwise velocity u in the spanwise direction at various x-locations at $y = 0.7426$ and $Re = 397$. Comparisons are made with the results of Armaly *et al.* [3] and the two different codes (FEFLO and FEM3D) along with the corresponding two-dimensional values of FEM3D.

is consistently missing in the experimental data for the case of $Re = 397$. This fact has also been observed with the discussion of Figure 10. The numerical results in Figures 11–13 show a strong variation close to the lateral wall for both Reynolds numbers, which leaves the value of the streamwise velocity in the plane of symmetry unaffected. Although the experimental results show strong variations close to the lateral wall at $Re = 648$ as well, this phenomenon has been used to support the discrepancy of the two-dimensional calculations of Armaly *et al.* [3] with their measurements. However, the results of both codes show that the strong variations of the flow phenomena close to the lateral wall decay as the flow approaches the plane of symmetry (Figures 7–13), so that the deviations of the experimental results may be attributed to the omnipresent background noise or other issues inherent with the execution of laboratory experiments.

4.7. Shear stress distribution

The study of shear stress along the walls of the downstream channel is useful in the understanding of the relative strength of the eddies. Figure 14 depicts the dependence of shear stress on the streamwise location downstream of the step at the plane of symmetry at $Re = 800$ both along the lower and upper walls.

DOI: 10.1002/fld

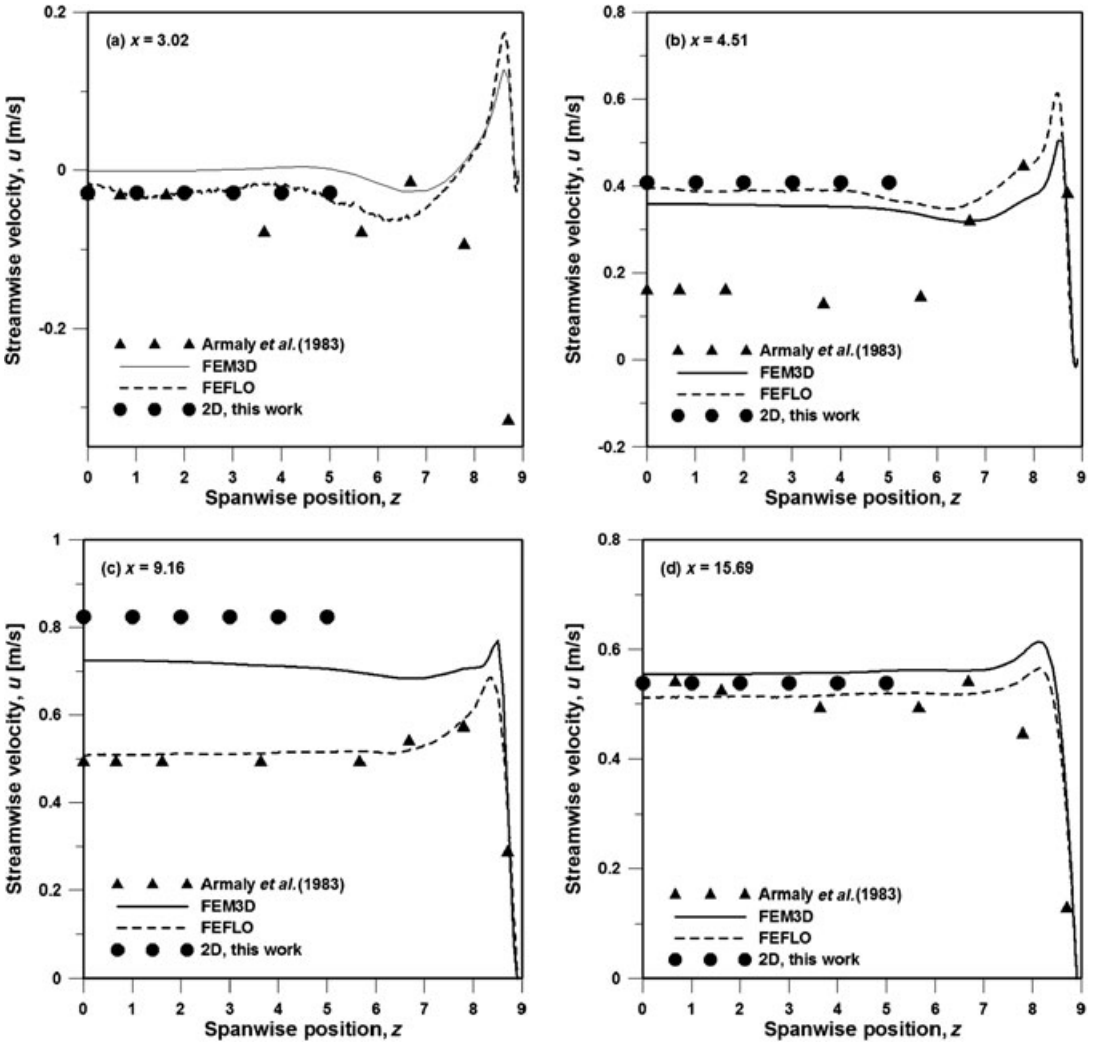

Figure 12. (a)–(d) Variation of streamwise velocity u in the spanwise direction at various x-locations at $y = 0.2327$ and $Re = 648$. Comparisons are made with the results of Armaly *et al.* [3] and the two different codes (FEFLO and FEM3D) along with the corresponding two-dimensional values of FEM3D.

The shear stress along the lower wall attains a global minimum at the vortex center of the eddy. Then, the shear stress grows monotonically until it attains a global maximum near the vortex center of the eddy on the upper wall. In this region, the net height of the channel for forward flow reaches a minimum, so that the rate of change in the streamwise velocity profile reaches a maximum. The shear stress drops then and reaches a local minimum in the region of reattachment of the upper eddy. There, it is expected that the flow is in its rearrangement phase to attain its one-dimensional parabolic profile. The flow undergoes some sort of sudden expansion, so that the rate of change of the streamwise velocity near the wall is smaller than in its fully developed one-dimensional configuration. Finally, the shear rate obtains its one-dimensional parabolic value as the flow proceeds to the outflow of the domain.

This distribution of shear stress along the lower wall of the step is characteristic of $Re \geqslant 700$. For $Re \leqslant 400$, there is no global maximum because the eddy along the upper wall is nonexistent. In the region $500 \leqslant Re < 700$, the maximum of the shear stress is a local one because the eddy along the upper wall is weak.

The shear stress along the upper wall attains a global maximum near the vortex center of the eddy, as expected. It is interesting to observe the sharp gradient of the shear stress right over the step and

DOI: 10.1002/fld

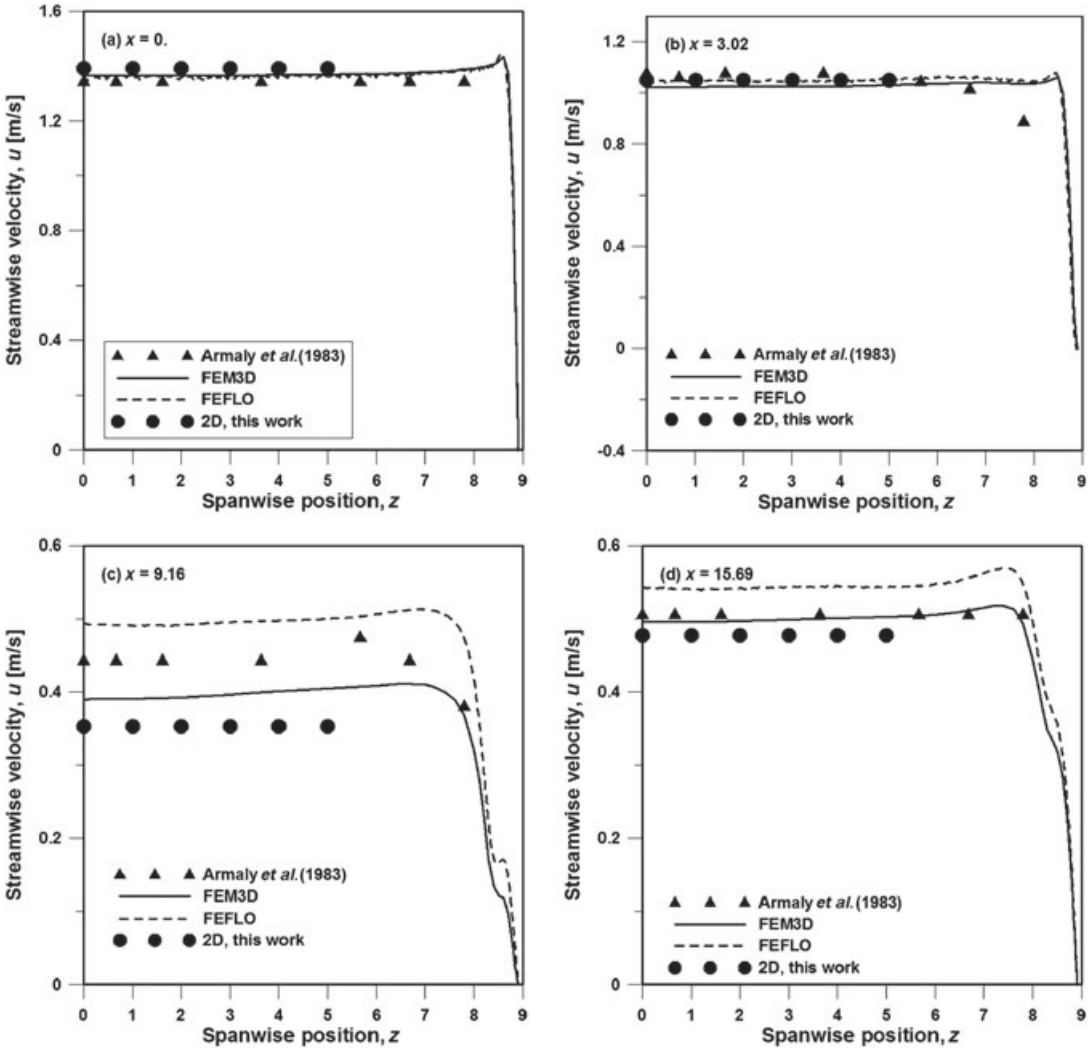

Figure 13. (a)–(d) Variation of streamwise velocity u in the spanwise direction at various x-locations at $y = 0.7426$ and $Re = 648$. Comparisons are made with the results of Armaly *et al.* [3] and the two different codes (FEFLO and FEM3D) along with the corresponding two-dimensional values of FEM3D.

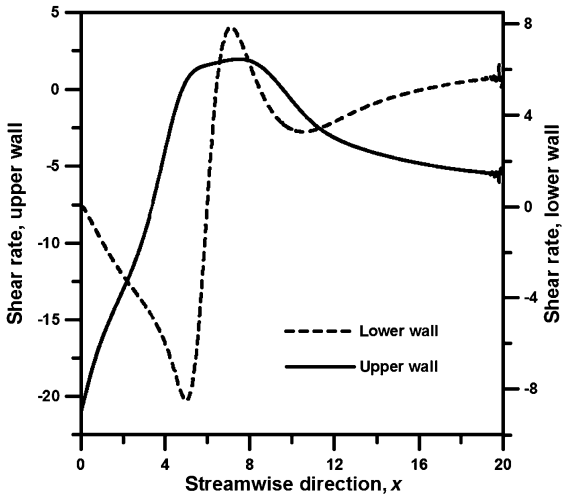

Figure 14. Calculated shear stress distribution along the lower and upper walls at $Re = 800$.

DOI: 10.1002/fld

its rapid monotonic decrease to zero at the detachment point of the eddy. The fact that the region around the maximum is relatively flat and that the absolute value of the maximum is low shows the weakness of this eddy compared with the eddy along the lower wall.

This is the reason why the eddy along the upper wall disappears at higher Reynolds numbers, as first observed by Armaly *et al.* [3]. However, this eddy adds to the complication of flow for as long as it appears, as discussed in the previous subsections, especially at the position of the detachment. The distribution of shear stress in Figure 14 along the upper wall is characteristic of all Reynolds number studied. It should be noted, though, that for $Re \leqslant 400$ the global maximum is a negative number, as the eddy is nonexistent.

It is interesting to compare the three-dimensional results of this work with the two-dimensional ones, with regard to the values of the global extrema and their corresponding positions. The results are given in Tables V and VI. It should be noted that the deviation of the three-dimensional computations, regarding the magnitude of shear stress, from the two-dimensional ones is defined as $|x - y| / y$ with x the three-dimensional results and y the two-dimensional result.

Regarding the main recirculation region along the lower wall, it is observed that the location of the global minimum of the three-dimensional computations deviates less than 5% from the two-dimensional results in all Reynolds numbers studied apart from $Re = 700$ and $Re = 800$ where the deviation is 5.6% and 7.7%, respectively (Table V). The deviation of the magnitude of the global minimum is less than 5% in the regions $100 \leqslant Re \leqslant 500$ and $900 \leqslant Re \leqslant 1050$. The deviation increases slightly in the region $600 \leqslant Re \leqslant 800$ (up to 8.5% at $Re = 700$).

Regarding the position of the global maximum along the lower wall, the deviation is less than 22% in the whole range of Reynolds numbers. Actually, the deviation decreases monotonically

Table V. Shear stress $\partial u / \partial y$, lower wall, results of this work.

Re	3D computations global minimum/ x-position	2D computations global minimum/ x-position	3D computations global maximum/ x-position	2D computations global maximum/ x-position
100	−4.5078/0.7291	−4.4923/0.7286	—	—
200	−5.4023/1.3514	−5.4109/1.3552	—	—
300	−5.7997/2.0455	−5.8748/2.0549	—	—
400	−6.1019/2.6933	−6.2752/2.7120	—	—
500	−6.4412/3.3578	−6.7612/3.3743	—	—
600	−6.9282/4.0224	−7.4244/4.0131	—	—
648	−7.2474/4.2668	−7.8509/4.2445	—	6.7039/6.3692
700	−7.6507/4.5238	−8.3039/4.4679	6.5675/6.7620	7.3804/6.5481
800	−8.6613/4.9596	−9.2975/4.8826	8.0825/7.0522	8.7790/6.8820
900	−9.9237/5.2942	−10.3809/5.2617	9.7259/7.2757	10.1413/7.1600
1000	−11.1799/5.6278	−11.4635/5.6268	11.1761/7.4959	11.3841/7.4651
1050	−11.7074/5.7155	−12.0109/5.7351	11.7240/7.5850	11.9742/7.5786

Table VI. Shear stress $\partial u / \partial y$, upper wall, results of this work.

Re	3D computations global maximum/x-position	2D computations global maximum/x-position
100	−3.9180/1.7628	−3.8685/1.7645
200	−2.2039/2.5836	−2.1302/2.5678
300	−1.0795/3.4000	−0.9402/3.4024
400	−0.2143/4.2000	0.0025/4.2000
500	0.5099/5.0000	0.7719/5.0000
600	1.1144/5.7531	1.3589/5.8000
648	1.3607/6.1307	1.5916/6.2038
700	1.6012/6.6000	1.7994/6.6940
800	2.0086/7.4897	2.1669/7.5712
900	2.3426/8.2879	2.4763/8.3640
1000	2.5686/9.0305	2.7331/9.1270
1050	2.6218/9.3370	2.8441/9.5038

DOI: 10.1002/fld

from 21.4% (at $Re = 600$) to 0.6% (at $Re = 1050$). The deviation in the magnitude of the global maximum is again highest at $Re = 700$ and $Re = 800$ (11.7% and 12.4%, respectively). The deviation decreases from 8.6% at $Re = 800$ to 2.13% at $Re = 1050$. Overall, the deviation of the three-dimensional calculations from the two-dimensional ones is in most cases less than 10% for the magnitude of the extrema and less than 22% for their corresponding position, so that the results for the shear stress of the three-dimensional numerical experiment of this work may be regarded as two-dimensional in the plane of symmetry.

The comparison of the three-dimensional results with the two-dimensional calculations for the eddy along the upper wall shows a deviation of less than 10% in the whole range of Reynolds numbers studied for the position of the global maximum with the exception of $Re = 1050$ where the deviation is 16.7% (Table VI). The comparison in the magnitude of the shear stress yields higher discrepancies. The highest deviations are observed at $Re = 400$ (100%) and at $Re = 500$ (51.4%). This result may be surprising because such high deviations are the exception in the comparisons for the magnitude of shear stress made so far. It has been argued before though that the eddy along the upper wall is a weak one. This eddy appears around $Re \approx 400$. It is expected that a three-dimensional calculation may show its highest deviation in this parameter region where the inception of the eddy occurs.

It is interesting that there is no deviation in the position of the global maximum in the range $400 \leqslant Re \leqslant 500$. This fact verifies the accuracy of the three-dimensional calculations and shows that some fine features of a strictly two-dimensional flow, like the extrema of the shear stress, are almost impossible to be captured even by the most accurate three-dimensional simulation. The deviation in the magnitude of shear stress is relatively high at $Re = 300$ (12.9%), $Re = 600$ (22%), and $Re = 700$ (12.4%) compared with what has been reported so far regarding discrepancies in the magnitude of shear stress.

This result enhances the previous discussion regarding susceptibility to deviations because of the inception of the eddy rather than suggests three-dimensional effects because high deviations are observed even at $Re = 300$, where everybody agrees in the literature that the flow is at least two-dimensional up to $Re = 400$. The deviation in the magnitude of the shear stress drops to less than 8% in the region $800 \leqslant Re \leqslant 1050$ where the eddy is relatively strong and can be detected by three-dimensional calculations equally accurately as with two-dimensional computations.

5. CONCLUSIONS

The three-dimensional laminar backward-facing step flow has been studied in a computational domain that mimics actual laboratory conditions. The Reynolds number range was $100 \leqslant Re \leqslant 1050$. The geometry chosen was that of the test section introduced by Armaly *et al.* [3], who have performed some of the most cited laboratory experiments on this subject. Two finite element codes were used to solve the steady-state Navier–Stokes equations in order to enhance the credibility of the results. Several comparisons have also been performed in order to check the deviation of the three-dimensional computations from the ideal two-dimensional numerical experiment.

It is reported for the first time that a three-dimensional numerical experiment can predict the eddy along the upper wall of the channel upstream of the step under the laboratory experimental conditions of Armaly *et al.* [3].

The results for the reattachment position of the eddy along the lower wall and the detachment and reattachment positions of the eddy along the upper wall have been compared with two-dimensional computations. The comparison shows that the high aspect ratio of 1:36.7 yields two-dimensional results in the plane of symmetry of the computational domain for all three positions and for every Reynolds number studied. The highest deviation has been observed for the detachment position of the eddy along the upper wall at $Re = 600$. These are the first three-dimensional computations for this flow that are so close to two-dimensional calculations. The results are in accordance with a fundamental conclusion of De Brederode and Bradshaw [8, p. 33] who suggested an aspect ratio of 1:30 for negligible wall effects.

DOI: 10.1002/fld

The effects of lateral walls have been studied by computing streamlines in planes parallel and perpendicular to the walls. It has been shown that the flow attributes are distorted very close to the wall and assume their two-dimensional configuration in spanwise positions close to the symmetry plane. Computations of shear stress distributions verify the two-dimensional configuration of the flow in the plane of symmetry. The high deviation of the three-dimensional computations has been observed in the global maximum of the shear stress along the upper wall at $400 \leqslant Re \leqslant 500$, where the inception of the eddy occurs.

The calculation of the eddy along the upper wall, in conjunction with the agreement between three-dimensional and two-dimensional computations, has given the opportunity for a reevaluation of the conclusions that have been made so far in the literature regarding the laboratory experiments. It has been shown that the deviation of the measurements with respect to two-dimensional computations is from 21.4% (at $Re = 500$) up to two units of height (at $Re = 1050$) with regard to the detachment position and up to one unit of height with regard to the reattachment position of the eddy along the upper wall in the whole range of Reynolds numbers.

The good agreement of the experimental data with the two-dimensional and three-dimensional computations regarding the reattachment position of the eddy along the upper wall shows that laboratory experiments with aspect ratios higher than 36 reveal two-dimensional attributes in the plane of symmetry with a deviation of less than half the unit of height for most Reynolds numbers. The most vulnerable position of experimental data with respect to accuracy of measurement is the position of the detachment of the secondary eddy.

In the near future, it seems possible that the tremendous increase of computational power may permit the study of the direct numerical simulation of turbulence in domains with lateral walls rather than the use of periodic boundary conditions in the spanwise direction as is common practice today. In that respect, the results of this work may serve in testing appropriate numerical methods for such applications.

ACKNOWLEDGEMENT

N.A. Malamataris wishes to thank Dr. G. Brook of NICS at ORNL, J. Leveque of Cray at ORNL and J. O'Dell of SGI for useful discussions regarding issues of parallelization of FEM3D. Financial support for N.A. Malamataris to develop his three-dimensional parallel direct solver has been provided by the Technological and Educational Institute of W. Macedonia. This research was supported by allocation CTS080031 of advanced computing resources provided by the National Science Foundation. The computations were performed on Kraken (a Cray XT5) at the National Institute for Computational Sciences and on BlueGene/L at the National Center for Atmospheric Research. Additional computations have been performed on the SGI ICE machine at George Mason University.

REFERENCES

1. Schäfer F, Breuer M, Durst F. The dynamics of the transitional flow over a backward-facing step. *Journal of Fluid Mechanics* 2009; **623**:85–119.
2. Le H, Moin P, Kim J. Direct numerical simulation of turbulent flow over a backward-facing step. *Journal of Fluid Mechanics* 1997; **330**:349–374.
3. Armaly BF, Durst F, Pereira JCF, Schönung B. Experimental and theoretical investigation of backward-facing step flow. *Journal of Fluid Mechanics* 1983; **127**:473–496.
4. Adams EW, Johnston JP. Effects of the separating shear layer on the reattachment flow structure. Part 2. Reattachment length and wall shear stress. *Experiments in Fluids* 1988; **6**:493–499.
5. Lee T, Mateescu D. Experimental and numerical investigation of 2-D backward-facing step flow. *Journal of Fluids and Structure* 1998; **12**:703–716.
6. Tylli N, Kaiktsis L, Ineichen B. Sidewall effects in flow over a backward-facing step experiments and numerical simulations. *Physics of Fluids* 2002; **14**:3835–3845.
7. Erturk E. Numerical solutions of 2-D steady incompressible flow over a backward-facing step. Part I: high Reynolds number solutions. *Computers & Fluids* 2008; **37**:633–655.
8. De Brederode V, Bradshaw P. Three-dimensional flow in nominally two-dimensional separation bubbles. Flow behind a rearward-facing step. *Aero Report 72-19*, 1972. Imperial College of Science and Technology, London.
9. Williams PT, Baker AJ. Numerical simulations of laminar flow over a 3D backward-facing step. *International Journal of Numerical Methods in Fluids* 1997; **24**:1124–1183.

DOI: 10.1002/fld

10. Nie JH, Armaly BF. Reverse flow regions in three-dimensional backward-facing step flow. *International Journal of Heat and Mass Transfer* 2004; **47**:4713–4720.
11. Chiang TP, Sheu TWH. A numerical revisit of backward-facing step flow problem. *Physics of Fluids* 1999; **11**:862–874.
12. Biswas G, Breuer M, Durst F. Backward-facing step flows for various expansion ratios at low and moderate Reynolds numbers. *Journal of Fluids Engineering* 2004; **126**:362–374.
13. Barbosa Saldana JG, Anand NK, Sarin V. Forced convection over a three-dimensional-backward facing step. *International Journal for Computational Methods in Engineering Science and Mechanics* 2005; **6**:225–234.
14. Kitoh A, Sugawara K, Yoshikawa H, Ota T. Expansion ratio effects on three-dimensional separated flow and heat transfer around backward-facing steps. *Journal of Heat Transfer* 2007; **129**:1141–1155.
15. Nie JH, Chen YT, Hsieh HT. Effects of a baffle on separated convection flow adjacent to backward-facing step. *International Journal of Thermal Sciences* 2009; **48**:618–625.
16. Romé C, Glockner S, Caltagirone JP. Resolution of the Navier–Stokes equations on block structured grids. *International Journal for Numerical Methods in Fluids* 2007; **54**:1239–1268.
17. Barton IE. A numerical study of flow over a confined backward-facing step. *International Journal for Numerical Methods in Fluids* 1995; **21**:653–665.
18. Kim J, Moin P. Applications of a fractional-step method to incompressible Navier–Stokes equations. *Journal of Computational Physics* 1985; **83**:308–323.
19. Gartling DK. A test problem for outflow boundary conditions—flow over a backward-facing step. *International Journal for Numerical Methods in Fluids* 1990; **11**:953–967.
20. Papanastasiou TC, Malamataris N, Ellwoodm K. A new outflow boundary condition. *International Journal for Numerical Methods in Fluids* 1992; **14**:587–608.
21. Zienkiewicz OC, Taylor RL. *The Finite Element Method* (5th edn). Butterworth-Heinemann: Oxford, 2000.
22. Colonius T. Modeling artificial boundary conditions for compressible flows. *Annual Review of Fluid Mechanics* 2004; **36**:315–345.
23. Sayag R, Tziperman E. Spatiotemporal dynamics of ice streams due to a triple-valued sliding law. *Journal of Fluid Mechanics* 2009; **640**:483–505.
24. Gresho PM, Sani RL. *Incompressible Flow and the Finite Element Method*. J. Wiley & Sons Ltd.: Hoboken, 1998.
25. Owen DRJ, Hinton E. *Finite Elements in Plasticity: Theory and Practice*. Pineridge Press Ltd.: Swansea, 1980.
26. Irons BM. A frontal solution program for finite element analysis. *International Journal for Numerical Methods in Engineering* 1970; **2**:5–32.
27. Hood P. Frontal solution program for unsymmetric matrices. *International Journal for Numerical Methods in Engineering* 1976; **10**:379–399.
28. Löhner R. Renumbering strategies for unstructured grid solvers operating on shared memory, cache-based parallel machines. *Computer Methods in Applied Mechanics and Engineering* 1998; **163**:95–109.
29. Ramamurti R, Löhner R. A parallel implicit incompressible flow solver using unstructured meshes. *Computers and Fluids* 1996; **5**:119–132.
30. Löhner R. *Applied CFD Techniques*. J. Wiley & Sons Ltd.: Hoboken, 2008.
31. Löhner R. Multistage explicit advective prediction for projection-type incompressible flow solvers. *Journal of Computational Physics* 2004; **196**:143–152.
32. Löhner R, Chi Yang JR, Cebral JR, Camelli F, Soto O, Waltz J. Improving the speed and accuracy of projection-type incompressible flow solvers. *Computer Methods in Applied Mechanics and Engineering* 2006; **195**:3087–3109.
33. Soto O, Löhner R, Camelli F. A linelet preconditioner for incompressible flows. *International Journal of Numerical Methods for Heat and Fluid Flow* 2003; **13**:133–147.
34. Löhner R. Projective prediction of pressure increments. *Communications in Numerical Methods in Engineering* 2005; **21**:201–207.
35. Osswald GA, Ghia KN, Ghia U. *AIAA, Sixth CFD Conference*, Danvers, MA, 1983; 686–696.
36. Kaiktsis L, Karniadakis GEM, Orszag SA. Onset of three dimensionality, equilibria and early transition in flow over a backward facing step. *Journal of Fluid Mechanics* 1991; **231**:501–528.
37. Park H, Jeon W, Choi H, Yoo JY. Mixing enhancement behind a backward-facing step using tabs. *Physics of Fluids* 2007; **19**:105103.

DOI: 10.1002/fld